Adaptive Sliding-Mode-Based Speed Control in Finite Control Set Model Predictive Torque Control for Induction Motors

Yanqing Zhang, *Member, IEEE*, Zhonggang Yin, *Member, IEEE*, Wei Li, Jing Liu, and Yanping Zhang

***Abstract*—The conventional model predictive torque control (MPTC) for induction motor drives evaluates the electromagnetic torque and stator flux linkage in the cost function. However, in the speed outer loop design, the torque reference in the cost function generally utilizes a classic proportional-integral (PI) controller, which is not only dependent on motor parameters but also sensitive to the change of the load torque. In this article, an adaptive sliding-mode-control-based MPTC (ASMC-MPTC) method is proposed to improve the robustness of the finite control set model predictive control (FCS-MPC). First, the influence of the mismatched parameters for FCS-MPTC is introduced and the shortcoming of the PI-based MPTC (PI-MPTC) is analyzed. Then, a sliding-mode-control-based MPTC (SMC-MPTC) is studied, in which the exponential reaching law is introduced to control the trajectories of the state variables. To further improve the control performance of SMC-MPTC, the exponential reaching law is optimized to adjust the switching gain adaptively, thus the ASMC-MPTC is proposed. The PI-MPTC, SMC-MPTC, and ASMC-MPTC are compared theoretically and experimentally, and the results show that the proposed ASMC-MPTC has the best disturbance rejection ability and robustness against motor parameters variation and load torque change.**

***Index Terms*—Induction motor (IM), model predictive torque control (MPTC), robustness, sliding-mode control (SMC).**

Manuscript received June 17, 2020; revised September 21, 2020; accepted November 17, 2020. Date of publication December 3, 2020; date of current version March 5, 2021. This work was supported in part by the China Postdoctoral Science Foundation under Grant 2020M683524, in part by the Nature Science Basic Research Plan in Shaanxi Province under Grant 2020JQ-631, in part by the State Key Laboratory of Electrical Insulation and Power Equipment under Grant EIPE20201, in part by National Natural Science Foundation of China under Grant 51677150, in part by the State Key Laboratory of Large Electric Drive System and Equipment Technology under Grant SKLLDJ012016006, in part by the Key Research and Development Project of Shaanxi Province under Grant 2019GY-060, in part by the Key Laboratory of Industrial Automation in Shaanxi Province under Grant SLGPT2019KF01-12, in part by the Shaanxi Outstanding Youth Fund under Grant 2020JC-40, and in part by the Key Laboratory of Power Electronic Devices and High Efficiency Power Conversion in Xi'an under Grant 2019219814SYS013CG035. Recommended for publication by Associate Editor J. Zhang. *(Corresponding author: Zhonggang Yin.)*

Yanqing Zhang, Zhonggang Yin, and Yanping Zhang are with the School of Electrical Engineering, Xi'an University of Technology, Xi'an 710048, China (e-mail: zhangyanqing@xaut.edu.cn; zhgyin@xaut.edu.cn; zhangyanpingmao@126.com).

Wei Li is with the Veichi Electric Technology Co. Ltd., Suzhou 215000, China (e-mail: liwei19950426@163.com).

Jing Liu is with the Department of Electronic Engineering, Xi'an University of Technology, Xi'an 710048, China (e-mail: jingliu@xaut.edu.cn).

Color versions of one or more figures in this article are available at https://doi.org/10.1109/TPEL.2020.3042181.

Digital Object Identifier 10.1109/TPEL.2020.3042181

Nomenclature

$\boldsymbol{u}_s$	Stator voltage vector.
ψ_s and ψ_r	Stator flux linkage vector and rotor flux linkage vector.
$\boldsymbol{i}_s$ and $\boldsymbol{i}_r$	Stator current vector and rotor current vector.
T_e and T_L	Electromagnetic torque and load torque.
ω_e and ω_r	Electrical speed and mechanical speed.
L_s, L_r, and L_m	Stator, rotor, and mutual inductances.
R_s and R_r	Stator and rotor resistances.
n_p	Number of pole pairs.
J	Moment of inertia.
$\sigma(=1-L_m^2/L_sL_r)$	Leakage coefficient.
$T_r(=L_r/R_r)$	Rotor time constant.
T_s	Sampling period.
$*$	Denotes commanded values.
$\wedge$	Denotes estimated values.
$\sim$	Denotes the induction motor parameters used in the predictive process.

I. Introduction

MODEL predictive control (MPC) is becoming an attractive control method for power converters and motor drives [1], [2]. In recent years, it has become a popular research topic due to its easy implementation, multiobjective control, and easy inclusion of constraints and nonlinearities [3], [4]. Given that it eliminates the pulsewidth modulation, MPC achieves a faster dynamic response than that of the field-oriented control [2]. In addition, compared with the direct torque control, the voltage vector selected in MPC is more accurate and effective owing to the online optimization of a cost function [5]. In the field of electrical drives, MPC can be divided into two main categories: 1) continuous control set MPC (CCS-MPC), and 2) finite control set MPC (FCS-MPC) [5]. For the CCS-MPC method, it has a special case, which is called generalized predictive control [6]. The CCS-MPC can achieve a good control performance but it is complicated to apply and needs a pulsewidth modulator [7], [8]. Compared with CCS-MPC, FCS-MPC is simpler for handling various control objectives and constraints [9], [10]. By considering the model of the inverter used in the control system, FCS-MPC directly calculates all possible switching states and selects the optimal switching state based on the principle of minimizing the cost function [11]. Then the selected optimal

switching signal is output to the inverter directly without any modulators, and thus the drive system becomes simpler. Over the past decade, FCS-MPC has already been extensively used and investigated [12]–[14].

Finite control set model predictive torque control (FCS-MPTC) is a typical case of FCS-MPC, in which the stator flux linkages and electromagnetic torque are predicted as the state variables in the cost function. The switching state that minimizes the flux linkage and torque ripples the most is finally selected as the best voltage vector [15]. Then the optimal switching state directly applies to the inverter without modulators, and in the next sampling instant, the voltage vector produced by the inverter is applied to the motor [16]. FCS-MPTC is regarded as a very promising method and has many advantages, such as fast dynamics, straightforward structure, easy implementation, and the easy inclusion of constraints [17]. In recent years, the FCS-MPTC method has been widely studied [18], [19].

Although there are good prospects for the model predictive torque control (MPTC) method, some aspects should further be investigated to improve its practicability, such as robustness improvement [20]. It is well known that the MPC method is based on the established model, thus it naturally depends heavily on the motor parameters. Nevertheless, for the induction motors (IMs), the temperature will affect the stator resistance and rotor resistance, and the nonlinearity of the magnetic circuit will affect the mutual inductance. Thus it is necessary to improve the robust performance of MPTC, especially for the robustness against motor parameters variation. In [21], an immune-optimized disturbance observer-based MPCC method is presented, in which the robust performance against the motor parameters variation and step load disturbance have been enhanced. However, the presented method is complex, which will increase the computational burden. In [23], a novel disturbance controller is presented to estimate the inductance value in the MPCC-based system, and the parameter robustness of the SPMSM drive system has been improved. Nevertheless, the torque response can be further improved. For the encoderless FCS-MPTC drive system, a full-order sliding-mode observer is constructed [23], in which the stator resistance and rotor resistance online identifications are used to improve the robust performance. However, the chattering phenomenon needs to be further weakened. In [24], the linear disturbance observer-based MPTC control of the IM drive system is presented to suppress the mismatched parameters and load torque disturbances. Nevertheless, the added coordinate transformation in the presented method increases the complexity. In view of the uncertainty of permanent magnet synchronous motor (PMSM) and the inaccuracy of its model, which leads to the inaccuracy of its prediction performance, the predictive current control method is extended in [25] to improve the prediction accuracy. However, the verification of this method can be more comprehensive. In [14], a novel DOB-based robust predictive torque control method for the IM system has been studied. By utilizing the disturbance estimation technique, the load disturbance rejection ability and robustness have been improved. Nevertheless, the current response can be further improved. In [26], an active disturbance-rejection-based MPTC method has been presented to compensate for the torque prediction error produced by mismatched parameters, in which the robust performance has been enhanced. However, the parameter selection of the active disturbance rejection (ADR) algorithm is difficult.

Among the numerous motor control methods, the sliding-mode control (SMC) is one of the effective nonlinear robust control strategies. The SMC strategy has been successfully used for the power electronics system since it provides system dynamics with an invariance property to uncertainties once the system dynamics are controlled in the sliding mode. In [27], an SMC with a hysteresis control strategy is developed by combining the practical application of the multimode hybrid energy storage system, and thus the battery safety can be effectively ensured. In [27], a robust adaptive sliding-mode controller is designed for a boost converter with an unknown resistive load and external input voltage, and the presented method is robust with excellent recovery features to sudden input variations and unmodeled load variations. In [28], SMC is applied on multiple input/multiple output nonlinear systems, which allows chattering reduction on the control input while keeping a high tracking performance of the controller in the steady-state regime. To achieve the chattering-free control in theory, Wang *et al.* [29] have presented a high-order sliding-mode controller by shifting the discontinuous control to the derivative of the control law. However, it makes the sliding-mode controller more complicated and increases the computational burden.

In a variety of robust performance improvement methods, SMC is one of the effective nonlinear robust control strategies. The SMC strategy has been successfully used to improve the control performance of the drive system since it provides system dynamics with an invariance property to uncertainties once the system dynamics are controlled in the sliding mode. In addition, SMC also has the advantages of a simple structure and easy implementation. However, the chattering problem of SMC should be solved. In this article, aiming to improve the robust performance of FCS-MPTC on parameter uncertainties and load disturbances, an SMC-based MPTC (SMC-MPTC) is constructed, in which the exponential reaching law is introduced to control the trajectories of the state variables. Moreover, to further improve the control performance of SMC-MPTC, the exponential reaching law is optimized to adjust the switching gain adaptively, which is called the adaptive SMC-based MPTC (ASMC-MPTC). By using Lyapunov stability theory, the stability of the proposed ASMC-MPTC is analyzed in detail. The proportional-integral (PI) based MPTC (PI-MPTC), SMC-MPTC, and ASMC-MPTC are compared theoretically and experimentally, and the results show that the proposed ASMC-MPTC has the best disturbance rejection ability and robustness against motor parameters variation.

The rest of this article are summarized as follows. The mathematical models of IM and inverter are presented in Section II. Section III provides the analysis of mismatched parameters for PI-based FCS-MPTC. The proposed SMC-MPTC method is designed in Section IV, and the comparative analysis of the proposed ASMC-MPTC and conventional PI-MPTC is presented in Section V. The simulation results are presented in Section VI,

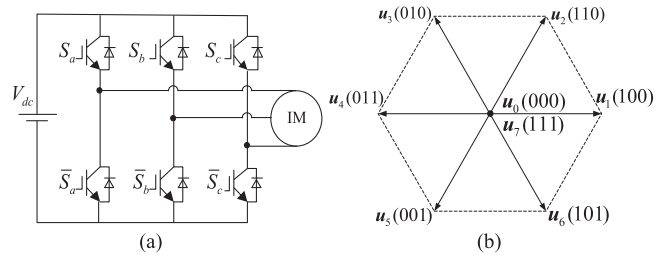

Fig. 1. (a) Two-level VSI circuit. (b) Voltage vectors.

and the implementation setup and experimental results are presented in Section VII. Finally, the conclusion of this article is presented in Section VIII.

II. Models of IM and Inverter

The state-space model of the IM in the stationary reference frame (α and β) can be described as follows:

$$\boldsymbol{u}_s = \boldsymbol{R}_s\boldsymbol{i}_s + \frac{d}{dt}\boldsymbol{\psi}_s \tag{1}$$

$$0 = \boldsymbol{R}_r\boldsymbol{i}_r + \frac{d}{dt}\boldsymbol{\psi}_r - j\omega_e\boldsymbol{\psi}_r \tag{2}$$

$$\boldsymbol{\psi}_s = L_s\boldsymbol{i}_s + L_m i_r \tag{3}$$

$$\boldsymbol{\psi}_r = L_r\boldsymbol{i}_r + L_m\boldsymbol{i}_s \tag{4}$$

$$T_e - T_L = \frac{J}{n_p}\frac{d\omega_r}{dt}. \tag{5}$$

Rearranging (1)–(5), the four-order nonlinear state-space model of the IM can be expressed as follows:

$$\dot{\boldsymbol{x}} = \boldsymbol{A}x + \boldsymbol{B}\boldsymbol{u} \tag{6}$$

$$A = \begin{bmatrix} -\left(\frac{\boldsymbol{R}_s}{\sigma L_s} + \frac{1}{\sigma T_r}\right)\boldsymbol{I} + \omega_r\boldsymbol{J} & \frac{1}{\sigma L_s}\left(\frac{1}{T_r}\boldsymbol{I} - \omega_r\boldsymbol{J}\right) \\ -\boldsymbol{R}_s\boldsymbol{I} & 0 \end{bmatrix} \tag{7}$$

$$B = \begin{bmatrix} \frac{1}{\sigma L_s}\boldsymbol{I} & \boldsymbol{I} \end{bmatrix}^T \tag{8}$$

where $x = [\,\boldsymbol{i}_s\ \boldsymbol{\psi}_s\,]^T$ and $u = [\,u_{s\alpha}\ u_{s\beta}\,]^T$.

The electromagnetic torque can be calculated as

$$T_e = 1.5n_p\Im m\left\{\boldsymbol{\psi}_s \cdot \boldsymbol{i}_s\right\}. \tag{9}$$

Fig. 1 shows the two-level voltage source inverter (VSI) circuit, in which the responding switching state $\boldsymbol{S}$ with every phase $\boldsymbol{S}_a$, $\boldsymbol{S}_b$, and $\boldsymbol{S}_c$ can be expressed as follows:

$$\boldsymbol{S} = \frac{2}{3}(\boldsymbol{S}_a + \boldsymbol{a}\boldsymbol{S}_b + a^2\boldsymbol{S}_c) \tag{10}$$

where $\boldsymbol{a} = e^{\,j2\pi/3}$. $\boldsymbol{S}_i$ represents the switches state, in which $\boldsymbol{S}_i = 1$ means ON and $\bar{S}_i = 0$ means OFF, where $i = a, b, c$. The relationship between the output voltage vector $\boldsymbol{u}_s$ of VSI and the switching state $\boldsymbol{S}$ can be described as

$$\boldsymbol{u}_s = \boldsymbol{V}_{dc}\boldsymbol{S} \tag{11}$$

where *V*dc is the dc bus voltage.

III. Analysis on the Robustness of PI-MPTC

A. Basic Principles of PI-MPTC Method

In the conventional PI-MPTC of IM drives, there are three primary parts of the FCS-MPTC method: the observation of stator flux linkage; the prediction of stator flux linkage and electromagnetic torque; and the minimization of the cost function. The detailed explanation can be as follows: the predictions of stator flux linkage $\boldsymbol{\psi}_s(k+1)$ and electromagnetic torque $T_e(k+1)$ should be carried out by each possible voltage vector. By using the forward Euler discrete equation, the predictions of the stator flux linkage and the stator current can be derived as

$$\boldsymbol{\psi}_s(k+1) = \boldsymbol{\psi}_s(k) + T_s(\boldsymbol{u}_s(k) - \boldsymbol{R}_s\boldsymbol{i}_s(k)) \tag{12}$$

$$\begin{aligned}\boldsymbol{i}_s(k+1) = &\left[1 - \left(\frac{\boldsymbol{R}_s}{\sigma L_s} + \frac{1}{\sigma T_r} - j\omega_r\right)T_s\right]\boldsymbol{i}_s(k) \\ &+ \frac{T_s}{\sigma L_s}\boldsymbol{u}_s(k)) \\ &+ \frac{T_s}{\sigma L_s}\left(\frac{1}{T_r} - j\omega_r\right)\boldsymbol{\psi}_s(k).\end{aligned} \tag{13}$$

Based on (12) and (13), the electromagnetic torque can be predicted as

$$T_e(k+1) = 1.5n_p\Im m\left\{\boldsymbol{\psi}_s(k+1) \cdot \boldsymbol{i}_s(k+1)\right\}. \tag{14}$$

B. Analysis of Parameters Mismatch for PI-MPTC

As mentioned above, the stator current and flux linkage predictions are calculated according to the discrete mathematical model of IM, making the FCS-MPTC prediction procedure dependent on motor parameters. To discuss the influence of parameters mismatch on the prediction accuracy of MPTC, some assumptions would be made: first, at *k* sampling instant, the stator current $\boldsymbol{i}_s(k)$ and the stator flux linkage $\boldsymbol{\psi}_s(k)$ are precise values; second, the stator leakage $L_{s\sigma}$ and the rotor leakage $L_{r\sigma}$ are constant.

The specific implementation can be described as: it is assumed that R_s and L_m are the actual parameters, and then $\boldsymbol{i}_s(k+1)$ and $T_e(k+1)$ are calculated by (12)–(14). $\tilde{R}_s$ and $\tilde{L}_m$ are the mismatched parameters, which are employed in the predictive process. Therefore, $\tilde{i}_s(k+1)$ and $\tilde{T}_e(k+1)$ based on the parameters mismatch are obtained in (15)–(17), where $\tilde{L}_s = \tilde{L}_m + L_{s\delta}$, $\tilde{L}_r = \tilde{L}_m + L_{r\delta}$, $\sigma = 1 - \tilde{L}_m^2/\tilde{L}_s\tilde{L}_r$, and $\tilde{T}_r = \tilde{L}_r/R_r$, respectively. The prediction errors of the stator current and the electromagnetic torque are defined as $\Delta\boldsymbol{i}_s = |\tilde{i}_s(k+1) - \boldsymbol{i}_s(k+1)|$ and $\Delta T_e = |\tilde{T}_e(k+1) - T_e(k+1)|$, respectively.

$$\begin{aligned}\tilde{i}_s(k+1) = &\left[1 - \left(\frac{\tilde{R}_s}{\tilde{\delta}\tilde{\sigma}\tilde{L}_s} + \frac{1}{\tilde{\sigma}\tilde{T}_r} - j\omega_r\right)T_s\right]\boldsymbol{i}_s(k) \\ &+ \frac{T_s}{\tilde{\sigma}\tilde{L}_s}\boldsymbol{u}_s(k)) + \frac{T_s}{\tilde{\sigma}\tilde{L}_s}\left(\frac{1}{\tilde{T}_r} - j\omega_r\right)\boldsymbol{\psi}_s(k)\end{aligned} \tag{15}$$

$$\tilde{\boldsymbol{\psi}}_s(k+1) = \boldsymbol{\psi}_s(k) + T_s(\boldsymbol{u}_s(k) - \tilde{R}_s\boldsymbol{i}_s(k)) \tag{16}$$

$$\tilde{T}_e(k+1) = 1.5n_p\Im m\left\{\tilde{\boldsymbol{\psi}}_s(k+1) \cdot \tilde{i}_s(k+1)\right\}. \tag{17}$$

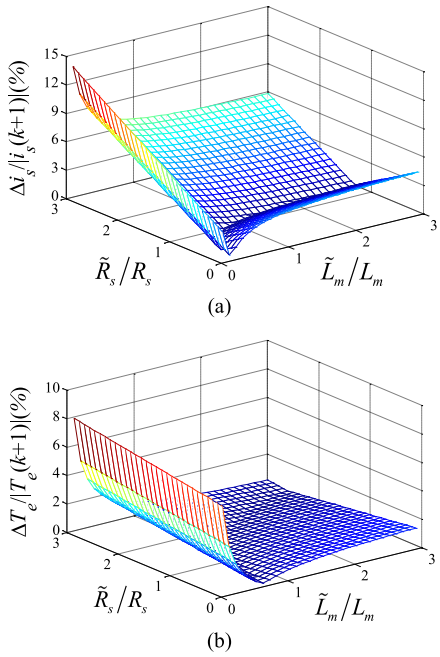

Fig. 2. (a) Prediction error of stator current with mismatched R_s and L_m at the rated speed and rated torque. (b) Prediction error of electromagnetic torque with mismatched R_s and L_m at the rated speed and rated torque.

Supposing that the IM operates at the rated speed with rated load and the direction of the stator flux linkage $\boldsymbol{\psi}_s$ coincides with the α-axis. According to the parameters of the IM used in this article, $\boldsymbol{i}_s = 4.1e^{j(\pi/3)}$ and $\boldsymbol{\psi}_s = 0.95e^{j0}$ are true at this time. It is known that there are seven different voltage vectors produced by a two-level VSI, which will result in a great number of cases for mismatched parameters analysis. To make the following analysis convenient, the one voltage vector selected maximizes prediction errors at k sampling instant. Fig. 2(a) shows the prediction error of the stator current when the stator resistance and mutual inductance are different from those true values. When $\tilde{L}_m/L_m = 1$ and $\tilde{R}_s/\boldsymbol{R}_s = 1$, the prediction error of the stator current is zero. Additionally, the stator current error is susceptible to mismatched mutual inductance. Compared with $\tilde{L}_m/L_m > 1$, the prediction error of the stator current is quite larger when $\tilde{L}_m/L_m < 1$. Fig. 2(b) reveals the prediction error of the torque with mismatched stator resistance and mismatched mutual inductance. It shows that the influences of parameters mismatch on the prediction error of stator current and the prediction error of torque have the same trends.

C. Analysis of Uncertain Disturbances for PI-MPTC

In order to analyze conveniently, Fig. 3 shows a simplified block diagram of the traditional PI-MPTC. The transfer function of the PI controller can be described as follows:

$$F(s) = k_p + \frac{k_i}{s} \tag{18}$$

where k_p and k_i are the proportional coefficient and the integral coefficient, respectively.

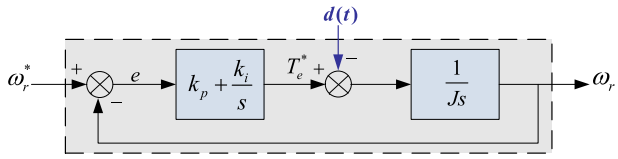

Fig. 3. Block diagram of the speed controller based on the PI controller.

The transfer function of IM can be described as

$$G(s) = \frac{1}{Js}. \tag{19}$$

As can be seen in Fig. 3, the transfer function $G_c(s)$ of the whole system can be derived as (20). Similarly from $d(t)$ to ω_r^*, the disturbance transfer function $G_d(s)$ can also be derived as (21)

$$G_c(s) = \frac{\omega_r(s)}{\omega_r^*(s)}|_{d(t)=0} = \frac{k_p}{J}\frac{s + (k_i/k_p)}{s^2 + (k_p/J)s + (k_i/J)} \tag{20}$$

$$G_d(s) = \frac{\omega_r(s)}{d(s)}|_{\omega_r^*=0} = -\frac{1}{J}\frac{s}{s^2 + (k_p/J)s + (k_i/J)}. \tag{21}$$

It can be seen that both the speed transient capacity and the disturbance rejection capacity rely on the denominator $s^2 + (k_p/J)s + (k_i/J)$. The standard form of the denominator can be described as

$$s^2 + 2\zeta\omega_0 s + \omega_0^2 \tag{22}$$

where $\zeta(\zeta = k_p/(2\sqrt{Jk_i}))$ is the damping ratio of the IM system and $\omega_0(\omega_0 = \sqrt{k_i/J})$ is the undamped natural frequency. When $0 < \zeta < 1$, the drive system operates in the underdamping state. $\zeta = 1$ dedicates that the drive system works in a critically damping state. When $\zeta > 1$, the drive system works in the overdamping state.

For the PI-MPTC controller, the load disturbance step $\Delta d(t)$ is taken into account for analyzing the disturbance rejection performance, and the integer error IE can be derived as

$$\mathrm{IE} = \int_0^\infty edt = -\lim_{s\to 0} G_d(s)\frac{\Delta d(t)}{s} = \frac{\Delta d(t)}{J}\left(\frac{2\zeta J}{k_p}\right)^2. \tag{23}$$

Based on the above-mentioned analysis, for better improving the antidisturbance ability, ζ should be smaller. However, if ζ is too small, it will result in the system instability. Therefore, for the traditional PI-MPTC controller, there must be a tradeoff in regard to the speed dynamic response and disturbance rejection capability.

IV. Design of ASMC-MPTC

According to the above-mentioned analysis, it can be seen that the conventional PI regulator has an inevitable tradeoff between the dynamic response and the disturbance rejection ability. In this article, unlike the linear controller or linear compensation strategy, a nonlinear controller, i.e., the sliding-mode controller is applied to improve the robust performance of FCS-MPTC on parameter uncertainties and load disturbance.

A. Basic Principles of SMC

The SMC is a kind of nonlinear control, which is based on the phase plane control [30]. By guiding the state trajectory of any point in space to a so-called sliding surface, SMC ensures the asymptotical stabliity of the motion system, and this motion process is called the sliding mode. In this article, for applying SMC into the speed regulator, the state variables x_1 and x_2 are designed as

$$\begin{cases} x_1 = \omega_r^* - \omega_r \\ x_2 = \dot{\boldsymbol{x}}_1 = -\dot{\omega}_r \end{cases} \tag{24}$$

where ω_r^* is the given speed.

Combining (5) and (24), it can be concluded

$$\begin{cases} \dot{\boldsymbol{x}}_1 = -\dot{\omega}_r = -(n_p/J)(T_e - T_L) \\ \dot{\boldsymbol{x}}_2 = -\ddot{\omega}_r = -(n_p/J)\dot{T}_e. \end{cases} \tag{25}$$

Assuming that $b = n_p/J$, $\tau = n_p T_L/J$, and $U = \dot{T}_e$, then (25) can be rewritten as

$$\begin{bmatrix} \dot{\boldsymbol{x}}_1 \\ \dot{\boldsymbol{x}}_2 \end{bmatrix} = \begin{bmatrix} 0 & 1 \\ 0 & 0 \end{bmatrix} \begin{bmatrix} x_1 \\ x_2 \end{bmatrix} + \begin{bmatrix} 0 \\ -b \end{bmatrix} U. \tag{26}$$

A first-order sliding-mode surface is selected as

$$s = cx_1 + x_2 \tag{27}$$

where s is the sliding-mode surface and c is the sliding-mode coefficient.

Normally for the SMC method, since the basic idea is to ensure that the control system satisfies the stability criteria, the reaching way of state variables to the sliding-mode surface also has a significant effect on the control performance. Thus to improve the control precision, the exponential reaching law is adopted as a typical reaching law to control the trajectories of the state variables, which is shown as [31]

$$\dot{s} = -\varepsilon \mathrm{sgn}(s) - ks \tag{28}$$

where ε is the switching gain with $\varepsilon > 0$ and k is the exponent coefficient with $k > 0$. Based on (25), (27), and (28), the torque reference T_e^* can be derived as

$$T_e^* = \frac{1}{b} \int [cx_2 + \varepsilon \mathrm{sgn}(s) + ks] dt. \tag{29}$$

B. Proposed ASMC

For the basic SMC-MPTC method, the values of ε and k in (29) will directly affect the dynamic performance. By integrating (28) from 0 to the reaching time t, with $s(t) = 0$, the reaching time t can be calculated as

$$t = \frac{|s(0)| - \left| \int_0^t \varepsilon s dt \right|}{k}. \tag{30}$$

It can be seen from (30) that by designing high values of ε and k, the reaching time t will be reduced, which means that the controller has a rapid speed response. Nevertheless, due to the inherent characteristic of SMC, the high values of ε and k will significantly aggravate the chattering phenomenon. Therefore, there exists a dilemma between the requirement of the chattering phenomenon reduction and fast dynamic response, and multiple factors, such as stability and rapidity, should be considered when designing the parameters of the exponential reaching law.

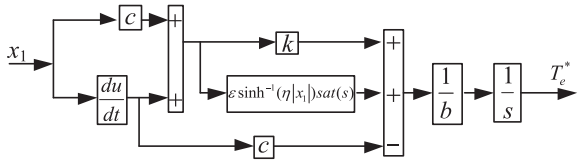

Fig. 4. Block diagram of the ASMC algorithm.

In this article, the ASMC-MPTC is proposed to solve the above-mentioned problem, in which the improved reaching law is designed as

$$\dot{s} = -\varepsilon \, sinh^{-1}(\eta \, |x_1|)\mathrm{sat}(s) - ks \tag{31}$$

where $\sinh^{-1}(\cdot)$ is the inverse hyperbolic sine function, x_1 is the state variable of ASMC, and $\lim_{t\to\infty} |x_1| = 0$, $\eta > 0$. It is known that the value of $\sinh^{-1}(\cdot)$ decreases with the decrease of the independent variable, and the closer the independent variable is to zero, the greater its slope will be. Based on this characteristic, the inverse hyperbolic sine function is very suitable for regulating the speed of the state variable reaching the sliding surface.

It is noted from (31) that if the state variables are far away from the sliding-mode surface, then a fast reaching speed is obtained. Moreover, as the state variables get closer to the sliding surface, the reaching speed gradually decreases from a large value to zero. Therefore, the proposed ASMC-MPTC can guarantee the rapidity and robustness of the controller, and suppress the chattering phenomenon at the same time. Moreover, the design range of the parameters in the ASMC algorithm is wider than that of the traditional SMC, and it needs to be considered and adjusted comprehensively in real implementation.

In addition, to further suppress the chattering phenomenon, the saturation function sat(·) is selected to replace the sign function sgn(·) in (28), and the saturation function is defined as

$$\mathrm{sat}(s) = \begin{cases} 1 & s > \Delta \\ k's & s \le \Delta, k' = 1/\Delta \\ -1 & s < -\Delta \end{cases} \tag{32}$$

where Δ is a positive constant. The basic principle of sat(·) can be expressed as: in the region represented by Δ, the linear feedback control is used. Outside the region represented by Δ, the switching control is used.

With the proposed ASMC-MPTC, the torque reference shown in (29) can be rewritten as

$$T_e^* = \frac{1}{b} \int [cx_2 + \varepsilon \, sinh^{-1}(\eta \, |x_1|)\mathrm{sat}(s) + ks] dt. \tag{33}$$

According to the aforementioned derivation, the design of the proposed ASMC algorithm can be described in Fig. 4.

C. Flux Linkage Estimation

To obtain accurate stator flux linkage information, an adaptive full-order observer is designed to estimate the stator flux linkage of the IM. The adaptive full-order observer is derived based on the IM model, which is shown as

$$\dot{\hat{\boldsymbol{x}}} = A\hat{x} + \boldsymbol{Bu} + \boldsymbol{G}(\boldsymbol{i}_s - \hat{\boldsymbol{i}}_s) \tag{34}$$

where $\hat{\boldsymbol{x}} = [\hat{\boldsymbol{i}}_s \quad \hat{\boldsymbol{\psi}}_s]^T$.

It is known that the gain matrix $\boldsymbol{G}$ plays a significant role in the adaptive full-order observer. Thus, a simplified design of the gain matrix $\boldsymbol{G}$ is expressed as [9]

$$G = -\begin{bmatrix} 2\mu \\ \mu/(\lambda L_m) \end{bmatrix} \tag{35}$$

where $\mu < 0$ and $\lambda = 1/(L_s L_r - L_m^2)$.

In the ASMC-MPTC algorithm, the predictions of stator flux linkage $\hat{\boldsymbol{\psi}}_s(k+1)$ and torque $\hat{T}_e(k+1)$ can be calculated by (12) and (14).

D. Design of Cost Function

In real-time implementations, the two-step prediction is used to eliminate the well-known one-step delay, thus the designed cost function is shown as

$$g = \left|T_e^* - \hat{T}_e(k+2)\right| + k_\psi \left||\psi_s^*| - \left|\hat{\psi}_s(k+2)\right|\right| \tag{36}$$

where k_ψ is the weighting factor, which increases or decreases the relative importance of the torque versus flux control in the MPTC system. If the same importance is assigned to both control objectives, this factor would correspond to the ratio between the nominal magnitudes of the torque T_n and stator flux $|\psi_{sn}|$, which is shown as

$$k_\psi = \frac{T_n}{|\psi_{sn}|}. \tag{37}$$

E. Proposed ASMC-MPTC

Fig. 5 shows the block diagram of the proposed ASMC-MPTC. As shown, the execution of the ASMC-MPTC algorithm includes two main steps: the predictions of the stator flux linkage and torque; and the minimization of the cost function. The ASMC determines the generation of the torque reference and it has a very important impact on the performance of MPTC since the torque reference plays an important role in the cost function.

For the implementation of the proposed ASMC-MPTC, Fig. 6 presents the overall flow diagram.

V. Comparison Between PI-MPTC and the Proposed ASMC-MPTC

A. Stability Analysis of ASMC-MPTC Method

In this article, the Lyapunov stability theory is used to prove the stability of the proposed ASMC-MPTC. According to the

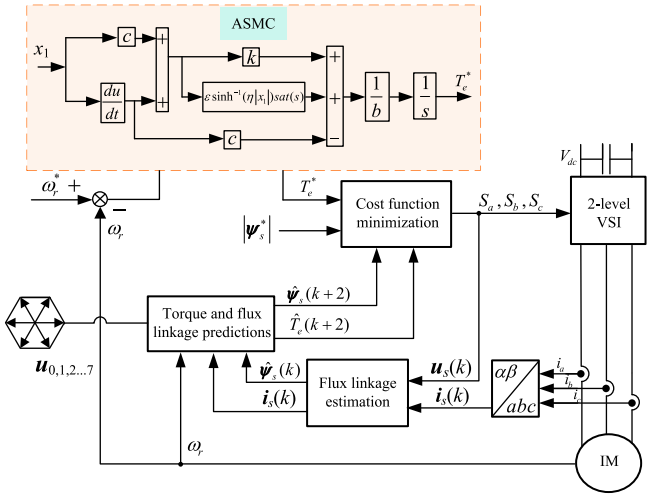

Fig. 5. Block diagram of ASMC-MPTC for IM systems.

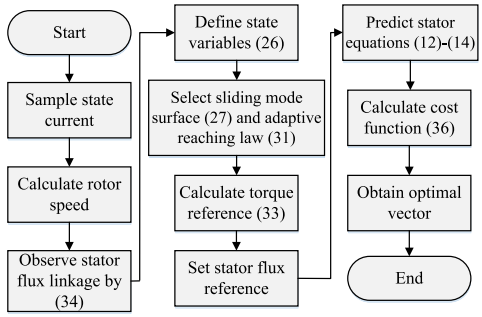

Fig. 6. Overall flow diagram of the proposed ASMC-MPTC.

Lyapunov stability theory, the Lyapunov function $V(\cdot)$ is designed as

$$V(x) = \frac{1}{2}s^2 \qquad s \neq 0. \tag{38}$$

Based on (38), it can be derived that

$$\dot{V}(x) = s\dot{s} \qquad s \neq 0. \tag{39}$$

Since the accessibility condition of the sliding-mode theory is that $s\dot{s} < 0$, then $\dot{V}(x) < 0$. Based on the Lyapunov stability theory, it can be concluded that the ASMC-MPTC system is asymptotical stable.

It is known from the sliding-mode theory that if the state variables reach the sliding-mode surface, then it can be obtained that

$$s = cx_1 + x_2 = cx_1 + \dot{x}_1 = 0. \tag{40}$$

By solving (40), it can be derived that

$$x_1 = \omega_r^* - \omega_r = C_0 e^{-\frac{t}{c}} \tag{41}$$

where C_0 is a constant. It is noted from (41) that when $t \to \infty$, then x_1 will tend to zero in the exponential form. Moreover, it shows that the system performance is mainly determined by c and it has nothing to do with the motor parameters and

disturbances. Hence, the proposed ASMC controller has a very good robust performance.

B. Comparison of PI-MPTC and ASMC-MPTC

When the PI-MPTC is adopted, T_e^* can be arranged as

$$T_e^* = k_p x_1 + k_i \left(\frac{1}{s} x_1\right). \tag{42}$$

In this case, it can be derived that

$$\ddot{x}_1 + bk_p \dot{x}_1 + bk_i x_1 - \tau = 0. \tag{43}$$

The comparison between PI-MPTC and ASMC-MPTC can be analyzed from the following three aspects.

1) Complexity of Parameter Tuning: It can be concluded that the PI-MPTC-based IM drives system is a second-order system according to (43). Therefore, as long as the PI-MPTC parameters (k_p and k_i) are designed properly, the control system will be stable. However, the design process of the PI-MPTC parameters is complicated for a second-order system. In ASMC-MPTC, the IM drive system is reduced to a first-order system according to (40) and the system stability only depends on the sliding-mode coefficient c. If c is designed appropriately, then the system will keep stable.

2) Complexity of Implementation: In comparison with (33) and (42), the expressions of the two controllers are similar. It is noted that ASMC-MPTC does not increase the complexity of the controller. The difference between the two controllers is that ASMC-MPTC is the variable structure control.

3) Disturbance Rejection Ability: When the external disturbance $d(t)$ occurs, it can be seen that the parameters of ASMC-MPTC can keep unchanged, and the system control performance will not be affected based on (33) and (40). However, for PI-MPTC, if the design parameters of the PI controller remain unchanged, the system control performance will be affected based on (43). Therefore, the ASMC-MPTC has a stronger robustness than PI-MPTC.

In the real implementation, it is difficult to ensure that the system moves along the sliding-mode line completely because of time delay, space delay, and other factors. However, the performance of ASMC is still better than that of the PI control. Compared with the PI control, ASMC is as simple as the PI control but it has better rapidity and robustness, which can realize higher performance control of IM.

VI. Simulation Results

In order to verify the performance of the proposed ASMC-MPTC, the simulations are carried out by MATLAB/Simulink. The tested IM parameters are given in Table I.

Fig. 7 shows the starting responses from 0 to 1500 r/min for PI-MPC and the proposed ASMC-MPTC methods. During the accelerating stage, the torque is limited to 150% rated value. At $t = 1.5$ s, an external load with the rated value is suddenly applied to the motor, the drops of the rotor speed are 94 and 47 r/min for PI-MPTC and ASMC-MPTC, respectively. Meanwhile, the recovery times are 0.32 and 0.13 s for PI-MPTC and ASMC-MPTC, respectively. It is clearly seen that the proposed ASMC-MPTC works better over a wide speed range and exhibits stronger robustness against the load disturbance.

TABLE I
Parameters of IM

parameter	value	parameter	value
rated power/kW	1.1	pole pair	2
rated voltage/V	380	J/kg·m^2	0.02
rated current/A	2.9	L_s/H	0.479
rated torque/N.m	7.45	L_r/H	0.479
R_s/Ω	5.27	L_m/H	0.421
R_r/Ω	5.07		

VII. Experimental Results

The PI-MPTC, SMC-MPTC, and the proposed ASMC-MPTC are tested on the same experimental test bench. The experimental system is shown in Fig. 8, and it can be seen that the system hardware consists of a 1.1 kW IM, an IM inverter, a loading system, and an oscillograph. A digital signal processor (TMS320F28335) is selected as the main processor, and the loading system consists of a PMSM and a servo inverter. Some experimental results are compared with the other robustness improvement methods of FCS-MPTC, which have been presented in [21] and [26].

A. Overall Performance of ASMC-MPTC

Fig. 9 shows the overall performance of the proposed ASMC-MPTC when the motor runs from standstill to 1500 r/min, in which the waveforms from top to bottom are rotor speed, stator current, torque, and stator flux linkage magnitude. As can be seen, the overshoot of the speed responses is nearly zero, and the electromagnetic torque ripple is very low. In addition, the stator current is smooth and sinusoidal in shape, and the stator flux linkage magnitude keeps stable. Therefore, Fig. 9 indicates that the motor exhibits a good steady and dynamic performance by using the proposed ASMC-MPTC method.

The ASMC-MPTC responses during the speed reversal at 1500 r/min are shown in Fig. 10, in which the waveforms from top to bottom are rotor speed, torque, stator flux linkage magnitude, and stator current. As shown, the motor accelerates and decelerates quickly in the reversal process, and the stator flux linkage magnitude of the proposed ASMC-MPTC method keeps constant. There are no oscillations of the stator current response in the process of motor speed reversal. It can be seen that the proposed ASMC-MPTC has a good dynamic performance during the speed reversal process.

The ASMC-MPTC responses during the speed reversal process are shown in Fig. 11, in which the waveforms from top to bottom are stator flux linkage in α, stator flux linkage in β, stator flux linkage magnitude response, and stator current response. As can be seen from the figure, the accurate stator flux linkage response is achieved in the whole range. In addition, the stator

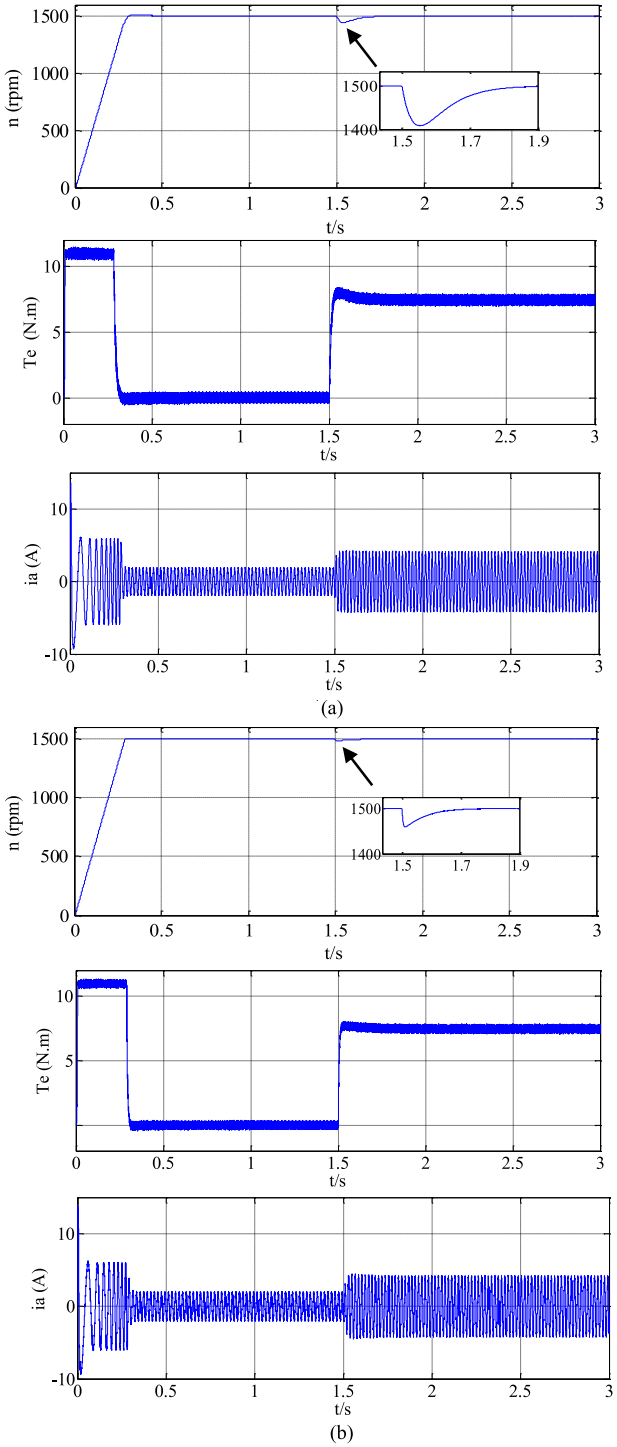

Fig. 7. Speed, torque, and stator current waveforms from standstill to 1500 r/min. (a) PI-MPTC. (b) ASMC-MPTC.

current response is smooth and without oscillations during the speed reversal process.

B. Dynamic Performance Comparison

To validate the disturbance rejection capability of the proposed ASMC-MPTC method, the experiments of step load

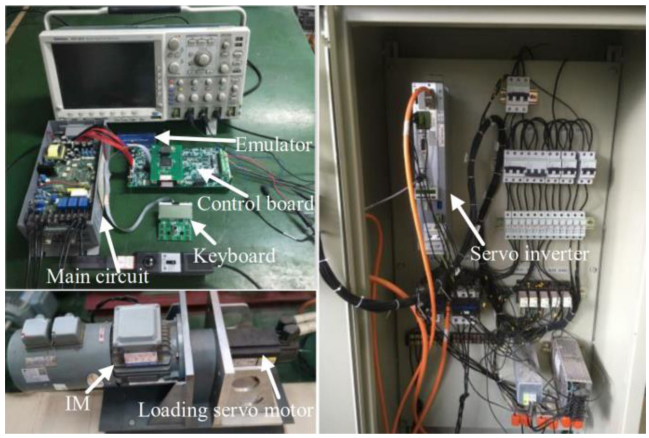

Fig. 8. Experimental platform.

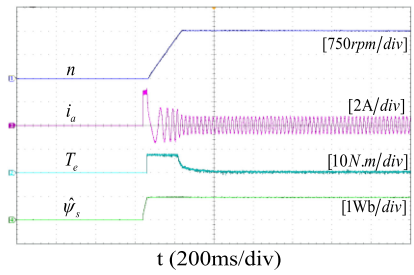

Fig. 9. ASMC-MPTC responses from standstill to 1500 r/min.

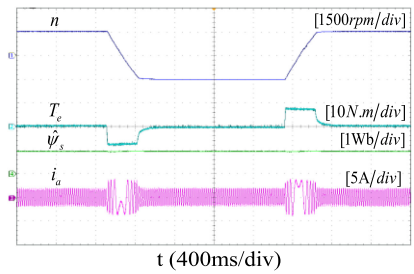

Fig. 10. ASMC-MPTC responses of speed reversal at 1500 r/min.

variations are performed. Fig. 12 shows the comparison at the speed of 1500 r/min with step rated load, in which the waveforms from top to bottom are rotor speed, torque reference, torque, and stator current. As shown, when the step load is suddenly added, the drops of the rotor speed are 295, 240, and 200 r/min for PI-MPTC, SMC-MPTC, and ASMC-MPTC, respectively. Meanwhile, the recovery times are 0.4, 0.28, and 0.14 s for PI-MPTC, SMC-MPTC, and ASMC-MPTC, respectively. It indicates that the proposed ASMC-MPTC has the best performance against the step load variations in the three methods and it is better than the ADR-MPTC method used in [26].

To verify the torque dynamic response of the proposed ASMC-MPTC method, the detailed experimental results of the torque response have been carried out in Fig. 13, in which the waveforms from top to bottom are torque reference and torque. As shown, when the step load torque is suddenly given from 0

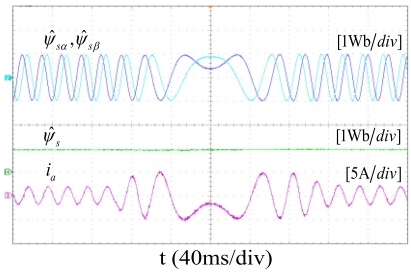

Fig. 11. ASMC-MPTC responses during a speed reversal process.

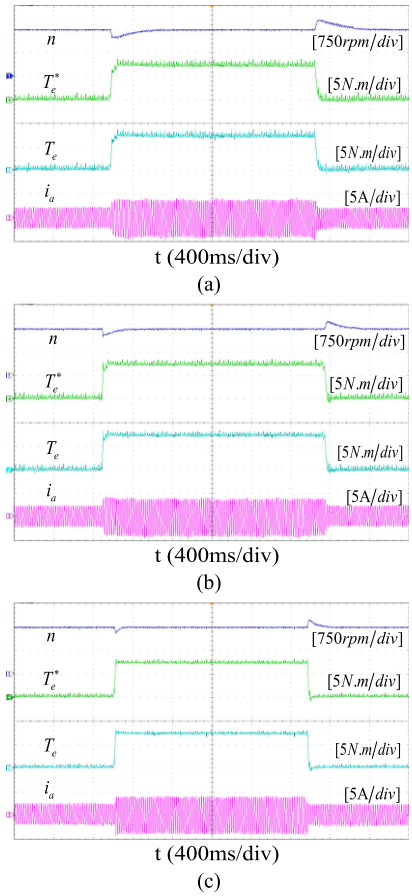

Fig. 12. Comparative results of dynamic response under the rated step load torque. (a) PI-MPTC. (b) SMC-MPTC. (c) ASMC-MPTC.

to the rated torque at 1500 r/min, the rising times of the torque response are 42, 32, and 18 ms for PI-MPTC, SMC-MPTC, and ASMC-MPTC, respectively. It shows that the proposed ASMC-MPTC has the fastest dynamic torque response in the three methods and it is better than the RPCC with DOB-IA method used in [21].

C. Parameter Sensitivity Comparison

In order to validate the robustness against motor parameters deviation based on PI-MPTC, SMC-MPTC, and the proposed ASMC-MPTC, the comparative results with $|\Delta R_s| = 30\%$ when the motor operates at 60 r/min are shown in Fig. 14, in which the

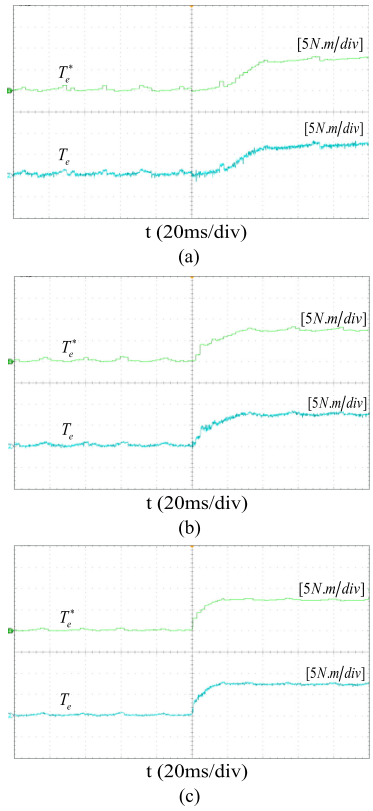

Fig. 13. Comparative results of electromagnetic torque dynamic response under the rated step load torque. (a) PI-MPTC. (b) SMC-MPTC. (c) ASMC-MPTC.

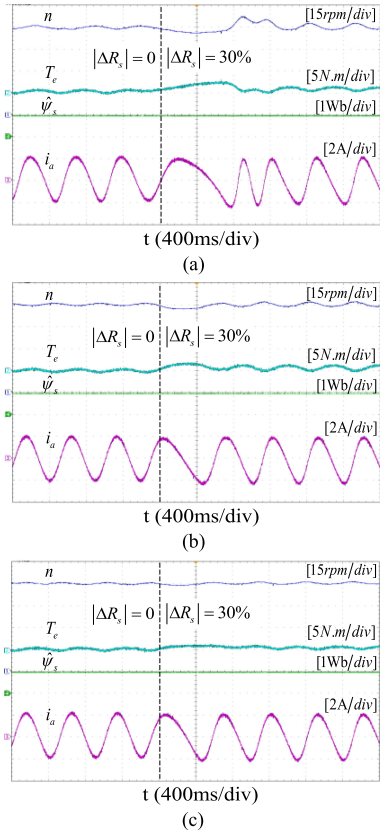

Fig. 14. Comparative results of robustness against R_s deviation in the low-speed range. (a) PI-MPTC. (b) SMC-MPTC. (c) ASMC-MPTC.

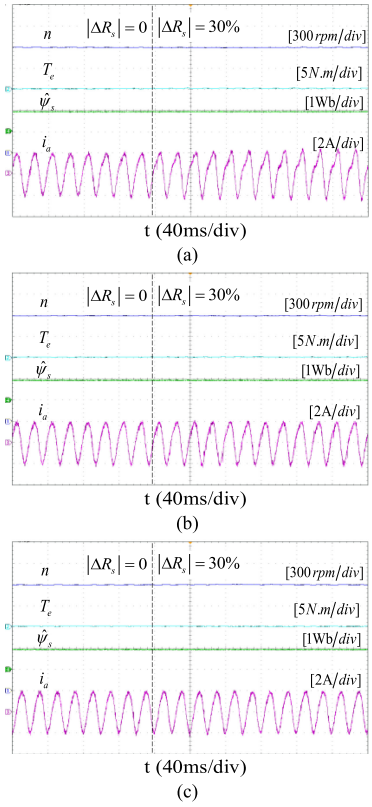

Fig. 15. Comparative results of robustness against R_s deviation in the high-speed range. (a) PI-MPTC. (b) SMC-MPTC. (c) ASMC-MPTC.

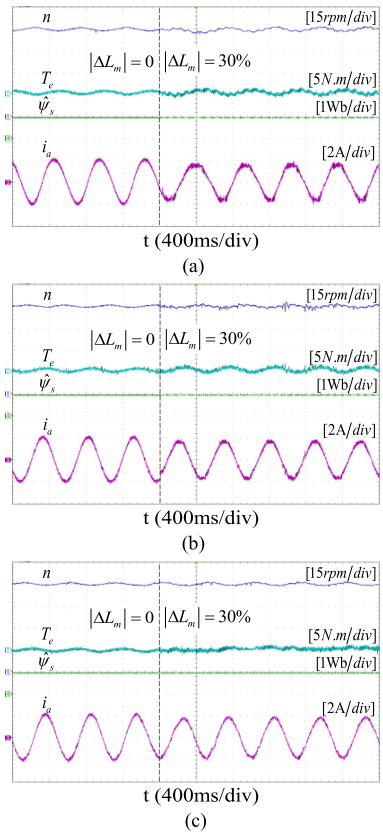

Fig. 16. Comparative results of robustness against L_m deviation in the low-speed range. (a) PI-MPTC. (b) SMC-MPTC. (c) ASMC-MPTC.

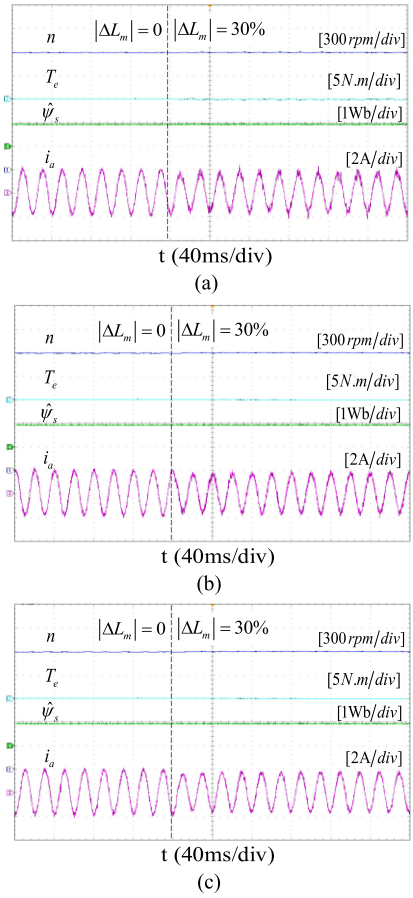

Fig. 17. Comparative results of robustness against L_m deviation in the high-speed range. (a) PI-MPTC. (b) SMC-MPTC. (c) ASMC-MPTC.

waveforms from the top to bottom are rotor speed, torque, stator flux linkage magnitude, and stator current. As shown, once R_s changes by 30%, then larger fluctuations of speed and torque occur, and the speed fluctuation and the torque ripple based on ASMC-MPTC is the lowest. For the stator current waveform, the oscillations have occurred for PI-MPTC. However, the waveforms based on SMC-MPTC and the proposed ASMC-MPTC keep smooth after R_s changes. In addition, the stator flux linkage magnitudes of the three methods keep stable after the resistance changes. It shows that the robust performance of the proposed ASMC-MPTC against R_s deviation is the strongest method.

For the robustness against $|\Delta R_s| = 30\%$ in the high-speed range, Fig. 15 shows the experimental result when the motor operates at 1500 r/min, in which the waveforms from top to bottom are rotor speed, torque, stator flux linkage magnitude, and stator current. As can be seen, once R_s changes by 30% in the high-speed range, all the three methods keep stable. However, the stator current becomes abnormal for PI-MPTC, and the stator current of the proposed ASMC-MPTC is the smoothest and the most sinusoidal in shape. In summary, Figs. 14 and 15 both show that the proposed ASMC-MPTC is the most robust against R_s deviation in the three methods.

Fig. 16 shows the comparative results with $|\Delta L_m| = 30\%$ when the motor operates at 60 r/min, in which the waveforms from top to bottom are rotor speed, torque, stator flux linkage

magnitude, and stator current. As shown, once L_m changes by 30%, then larger fluctuations of speed and torque occur, in which the speed fluctuation and the torque ripple based on ASMC-MPTC is the lowest. For the stator current, the oscillations have occurred into the stator current for all three methods. However, the stator current of the proposed ASMC-MPTC is the smoothest and the most sinusoidal in shape. In addition, the stator flux linkage magnitudes of the three methods keep stable after L_m changes. It is noted from Fig. 16 that when L_m changes, all the three methods can remain steady; nevertheless, the robust performance against L_m deviation based on the proposed ASMC-MPTC is the strongest.

For the robustness against $|\Delta L_m| = 30\%$ in the high-speed range, Fig. 17 shows the experimental result when the motor operates at 1500 r/min, in which the waveforms from top to bottom are rotor speed, torque, stator flux linkage magnitude, and stator current. As can be seen, once L_m changes by 30% in the high-speed range, then stator current amplitude becomes abnormal, in which the stator current of the proposed ASMC-MPTC is the smoothest and the most sinusoidal in shape. It can be concluded from Figs. 16 and 17 that the proposed ASMC-MPTC is the most robust against L_m deviation in the three methods.

VIII. Conclusion

An ASMC-MPTC is proposed in this article to improve the robustness of FCS-MPTC on parameter uncertainties and load disturbance. The major contributions of this article include the following.

1) The influence of the mismatched parameters for FCS-MPTC is introduced and the shortcoming of the conventional PI-MPTC is analyzed.

2) The SMC-MPTC is constructed, in which the exponential reaching law is introduced to control the trajectories of the state variables.

3) To further improve the control performance of SMC-MPTC, the exponential reaching law is optimized to adjust the switching gain adaptively, which is called ASMC-MPTC.

The PI-MPTC, SMC-MPTC, and ASMC-MPTC are compared theoretically and experimentally, and the results show that the proposed ASMC-MPTC has the best disturbance rejection ability and robust performance against motor parameters variation.

References

[1] A. Aliaskari, B. Zarei, S. A. Davari, F. Wang, and R. Kennel, "A modified closed-loop voltage model observer based on adaptive direct flux magnitude estimation in sensorless predictive direct voltage control of an induction motor," *IEEE Trans. Power Electron.*, vol. 35, no. 1, pp. 630–639, Jan. 2020.

[2] F. Wang, H. Xie, Q. Chen, S. A. Davari, J. Rodriguez, and R. Kennel, "Parallel predictive torque control for induction machines without weighting factors," *IEEE Trans. Power Electron.*, vol. 35, no. 2, pp. 1779–1788, Feb. 2020.

[3] J. Holtz, "Advanced PWM and predictive control—An overview," *IEEE Trans. Ind. Electron.*, vol. 63, no. 6, pp. 3837–3844, Jun. 2016.

[4] S. Vazquez, J. Rodriguez, M. Rivera, L. G. Franquelo, and M. Norambuena, "Model predictive control for power converters and drives: Advances and trends," *IEEE Trans. Ind. Electron.*, vol. 64, no. 2, pp. 935–947, Feb. 2017.

[5] M. Rivera, J. Rodriguez, and S. Vazquez, "Predictive control in power converters and electrical drives—Part I," *IEEE Trans. Ind. Electron.*, vol. 63, no. 6, pp. 3834–3836, Jun. 2016.

[6] P. Alkorta, O. Barambones, J. A. Cortajarena, and A. Zubizarrreta, "Efficient multivariable generalized predictive control for sensorless induction motor drives," *IEEE Trans. Ind. Electron.*, vol. 61, no. 9, pp. 5126–5134, Sep. 2014.

[7] B. Wang, Z. Dong, Y. Yu, G. Wang, and D. Xu, "Static-errorless deadbeat predictive current control using second-order sliding-mode disturbance observer for induction machine drives," *IEEE Trans. Power Electron.*, vol. 33, no. 3, pp. 2395–2403, Mar. 2018.

[8] B. Wang, X. Chen, Y. Yu, G. Wang, and D. Xu, "Robust predictive current control with online disturbance estimation for induction machine drives," *IEEE Trans. Power Electron.*, vol. 32, no. 6, pp. 4663–4674, Jun. 2017.

[9] H. Yang, Y. Zhang, P. D. Walker, J. Liang, N. Zhang, and B. Xia, "Speed sensorless model predictive current control with ability to start a free running induction motor," *IET Electr. Power Appl.*, vol. 11, no. 5, pp. 893–901, May 2017.

[10] F. Wang, J. Wang, R. M. Kennel, and J. Rodriguez, "Fast speed control of AC machines without the proportional-integral controller: Using an extended high-gain state observer," *IEEE Trans. Power Electron.*, vol. 34, no. 9, pp. 9006–9015, Sep. 2019.

[11] J. Wang, F. Wang, Z. Zhang, S. Li, and J. Rodriguez, "Design and implementation of disturbance compensation-based enhanced robust finite control set predictive torque control for induction motor systems," *IEEE Trans. Ind. Inform.*, vol. 13, no. 5, pp. 2645–2656, Oct. 2017.

[12] C. A. Rojas, J. R. Rodriguez, S. Kouro, and F. Villarroel, "Multiobjective fuzzy-decision-making predictive torque control for an induction motor drive," *IEEE Trans. Power Electron.*, vol. 32, no. 8, pp. 6245–6260, Aug. 2017.

[13] Z. Zhang, J. Rodriguez, and R. Kennel, "Advanced control strategies for direct-drive PMSG wind turbine systems: Direct predictive torque control approaches," *CPSS Trans. Power Electron. Appl.*, vol. 2, no. 3, pp. 217–225, Sep. 2017.

[14] M. Norambuena, J. Rodriguez, Z. Zhang, F. Wang, C. Garcia, and R. Kennel, "A very simple strategy for high-quality performance of AC machines using model predictive control," *IEEE Trans. Power Electron.*, vol. 34, no. 1, pp. 794–800, Jan. 2019.

[15] F. Wang, S. Li, X. Mei, W. Xie, J. Rodriguez, and R. M. Kennel, "Model-based predictive direct control strategies for electrical drives: An experimental evaluation of PTC and PCC methods," *IEEE Trans. Ind. Inform.*, vol. 11, no. 3, pp. 671–681, Jun. 2015.

[16] J. Rodriguez *et al.*, "State of the art of finite control set model predictive control in power electronics," *IEEE Trans. Ind. Inform.*, vol. 9, no. 2, pp. 1003–1016, May 2013.

[17] S. Vazquez *et al.*, "Model predictive control: A review of its applications in power electronics," *IEEE Ind. Electron. Mag.*, vol. 8, no. 1, pp. 16–31, Mar. 2014.

[18] Y. Zhang, B. Xia, and H. Yang, "Performance evaluation of an improved model predictive control with field oriented control as a benchmark," *IET Electr. Power Appl.*, vol. 11, no. 5, pp. 677–687, May 2017.

[19] P. Karamanakos and T. Geyer, "Guidelines for the design of finite control set model predictive controllers," *IEEE Trans. Power Electron.*, vol. 35, no. 7, pp. 7434–7450, Jul. 2020.

[20] X. Shi, J. Zhu, L. Li, and D. D.-C. Lu, "Model-predictive-based duty cycle control with simplified calculation and mutual influence elimination for AC/DC converter," *IEEE J. Emerg. Sel. Top. Power Electron.*, vol. 7, no. 1, pp. 504–514, Mar. 2019.

[21] Z. Yin, X. Han, C. Du, J. Liu, and Y. Zhong, "Research on model predictive current control for induction machine based on immune-optimized disturbance observer," *IEEE J. Emerg. Sel. Top. Power Electron.*, vol. 6, no. 4, pp. 1699–1710, Dec. 2018.

[22] X. Zhang, L. Zhang, and Y. Zhang, "Model predictive current control for PMSM drives with parameter robustness improvement," *IEEE Trans. Power Electron.*, vol. 34, no. 2, pp. 1645–1657, Feb. 2019.

[23] F. Wang *et al.*, "An encoderless predictive torque control for an induction machine with a revised prediction model and EFOSMO," *IEEE Trans. Ind. Electron.*, vol. 61, no. 12, pp. 6635–6644, Dec. 2014.

[24] J. Wang, F. Wang, G. Wang, S. Li, and L. Yu, "Generalized proportional integral observer based robust finite control set predictive current control for induction motor systems with time-varying disturbances," *IEEE Trans. Ind. Inform.*, vol. 14, no. 9, pp. 4159–4168, Sep. 2018.

[25] M. Siami, D. A. Khaburi, A. Abbaszadeh, and J. Rodriguez, "Robustness improvement of predictive current control using prediction error correction for permanent-magnet synchronous machines," *IEEE Trans. Ind. Electron.*, vol. 63, no. 6, pp. 3458–3466, Jun. 2016.

[26] L. Yan, F. Wang, M. Dou, Z. Zhang, R. Kennel, and J. Rodriguez, "Active disturbance-rejection-based speed control in model predictive control for induction machines," *IEEE Trans. Ind. Electron.*, vol. 67, no. 4, pp. 2574–2584, Apr. 2020.
[27] S. Oucheriah and L. Guo, "PWM-based adaptive sliding-mode control for boost DC–DC converters," *IEEE Trans. Ind. Electron.*, vol. 60, no. 8, pp. 3291–3294, Aug. 2013.
[28] C. J. Fallaha, M. Saad, H. Y. Kanaan, and K. Al-Haddad, "Sliding-mode robot control with exponential reaching law," *IEEE Trans. Power Electron.*, vol. 58, no. 2, pp. 600–610, Feb. 2011.
[29] B. Wang, C. Luo, Y. Yu, G. Wang, and D. Xu, "Antidisturbance speed control for induction machine drives using high-order fast terminal sliding-mode load torque observer," *IEEE Trans. Power Electron.*, vol. 33, no. 9, pp. 7927–7937, Sep. 2018.
[30] Y. Zhang, Z. Yin, Y. Zhang, J. Liu, and X. Tong, "A novel sliding mode observer with optimized constant rate reaching law for sensorless control of induction motor," *IEEE Trans. Ind. Electron.*, vol. 67, no. 7, pp. 5867–5878, Jul. 2020.
[31] W. Gao, Y. Wang, and A. Homaifa, "Discrete-time variable structure control systems," *IEEE Trans. Ind. Electron.*, vol. 42, no. 2, pp. 117–122, Apr. 1995.

Yanqing Zhang (Member, IEEE) received the B.S., M.S., and Ph.D. degrees in electrical engineering from the Xi'an University of Technology, Xi'an, China, in 2012, 2015, and 2019, respectively.

In 2019, he joined the School of Electrical Engineering, Xi'an University of Technology, Xi'an. His main research interests include the high-performance control of ac motor.

Zhonggang Yin (Member, IEEE) was born in Shandong, China, in 1982. He received the B.S., M.S., and Ph.D. degrees in electrical engineering from the Xi'an University of Technology, Xi'an, China, in 2003, 2006, and 2009, respectively.

In 2009, he joined the Electrical Engineering Department, Xi'an University of Technology, Xi'an, where he is currently a Professor. His research interests include the high-performance control of ac motor and digital control of power converters.

Wei Li was born in Weinan, China, in 1995. She received the B.S. and M.S. degrees in electrical engineering from the Xi'an University of Technology, Xi'an, China, in 2017 and 2020, respectively.

Since 2020, she has been an Engineer with Veichi Electric Technology Co., Ltd., Suzhou, China. Her main research interests include the high-performance control of ac motors.

Jing Liu was born in Anhui, China, in 1982. She received the B.S., M.S., and Ph.D. degrees in electronic engineering from the Xi'an University of Technology, Xi'an, China, in 2003, 2006, and 2009, respectively.

In 2009, she joined the Electronic Engineering Department, Xi'an University of Technology, Xi'an, where she is currently an Associate Professor. Her research interests include the power semiconductor devices and their application to power electronic devices.

Yanping Zhang was born in Shannxi, China, in 1989. He received the B.S. degree in electrical engineering from Xi'an Polytechnic University, Xi'an, China, in 2013, and the M.S. degree in power electronics and electrical drives in electrical engineering in 2017 from the Xi'an University of Technology, Xi'an, China, where he is currently working toward the Ph.D. degree.

His research interests include the high-performance sensorless control of PMSM.